HHS Public Access

Author manuscript

Mol Cancer Res. Author manuscript; available in PMC 2024 March 01.

Published in final edited form as:

Mol Cancer Res. 2023 September 01; 21(9): 867–880. doi:10.1158/1541-7786.MCR-22-1031.

Fibronectin contributes to a BRAF inhibitor-driven invasive phenotype in thyroid cancer through EGR1, which can be blocked by inhibition of ERK1/2.

Hannah M. Hicks[1], **Nikita Pozdeyev**[1,2], **Sharon B. Sams**[3], **Umarani Pugazhenthi**[1], **Elise S. Bales**[1], **Marie-Claude Hofmann**[4], **Logan R. McKenna**[1], **Rebecca E. Schweppe**[1,5]

[1]Division of Endocrinology, Metabolism, and Diabetes, Department of Medicine, University of Colorado School of Medicine, Aurora, Colorado 80045, USA.

[2]Department of Biomedical Informatics, University of Colorado School of Medicine, Aurora, Colorado 80045, USA

[3]Department of Pathology, Department of Medicine, University of Colorado School of Medicine, Aurora, Colorado, 80045, USA.

[4]Department of Endocrine Neoplasia and Hormonal Disorders – Research, Division of Internal Medicine, The University of Texas MD Anderson Cancer Center, Houston, Texas, 77030, USA.

[5]University of Colorado Cancer Center, University of Colorado School of Medicine, Aurora, Colorado, 80045, USA.

Abstract

Mutations in BRAF are common in advanced papillary and anaplastic thyroid cancer (PTC and ATC). However, *BRAF*-mutant PTC patients currently lack therapies targeting this pathway. Despite the approved combination of BRAF and MEK1/2 inhibition for patients with *BRAF*-mutant ATC, these patients often progress. Thus, we screened a panel of *BRAF*-mutant thyroid cancer cell lines to identify new therapeutic strategies. We showed that thyroid cancer cells resistant to BRAF inhibition (BRAFi) exhibit an increase in invasion and a pro-invasive secretome in response to BRAFi. Using Reverse Phase Protein Array (RPPA), we identified a nearly 2-fold increase in expression of the extracellular matrix protein, fibronectin, in response to BRAFi treatment, and a corresponding 1.8 to 3.0-fold increase in fibronectin secretion. Accordingly, the addition of exogenous fibronectin phenocopied the BRAFi-induced increase in invasion while depletion of fibronectin in resistant cells resulted in loss of increased invasion. We further showed that BRAFi-induced invasion can be blocked by inhibition of ERK1/2. In a BRAFi-resistant patient-derived xenograft model, we found that dual inhibition of BRAF and ERK1/2 slowed tumor growth and decreased circulating fibronectin. Using RNA-sequencing, we identified EGR1 as a top downregulated gene in response to combined BRAF/ERK1/2 inhibition, and we further showed that EGR1 is necessary for a BRAFi-induced increase in invasion and for induction of fibronectin in response to BRAFi.

Corresponding Author: Rebecca E. Schweppe, 12801 E. 17th Ave., # 1703 MS 8106, Research 1 South Aurora, CO 80045, 303-724-3921, Rebecca.Schweppe@cuanschutz.edu.

The authors declare no potential conflicts of interest.

Introduction

Advanced thyroid cancer including advanced papillary thyroid cancer (PTC) and anaplastic thyroid cancer (ATC) are commonly resistant to standard-of-care treatments, including radioiodine[1]. Accordingly, ATC is one of the most lethal human cancers, with a median overall survival of 9.4 months, depending on stage at the time of diagnosis[2]. Mutations in the MAP kinase (MAPK) pathway are common in PTC and ATC, especially *BRAF* with a prevalence of 40–60%[3]. Of these *BRAF* mutations, the most common is BRAF-V600E[3], which leads to constitutive activation of MAPK signaling[4]. Dabrafenib (BRAFi) and vemurafenib are ATP-competitive inhibitors that are selective for BRAF-V600E, making these inhibitors of clinical interest. However, patients with *BRAF*-mutated PTC or ATC experience disease progression on BRAF inhibitor monotherapy, which occurs either due to intrinsic (upfront) or acquired (occurring over a long time period) resistance[5]. To achieve more robust and sustained inhibition of the MAPK pathway, clinical trials have treated PTC and ATC[6] patients with upfront combination therapies of BRAF and MEK1/2 inhibition[7] (NCT02034110, NCT01723202). However, acquired resistance remains a significant clinical problem[8]. While rare, recent studies show transformation of PTC into ATC in response to combined BRAF and MEK1/2 inhibition[9]. Therefore, more durable, targeted therapeutic strategies are needed to circumvent drug resistance in patients with PTC or ATC. As the most downstream node of the MAPK pathway, ERK1/2 is an attractive therapeutic target. ERK1/2 inhibitors have been shown to have activity in models of BRAF- and MEK1/2-inhibitor resistance[10], and we previously found inhibiting ERK1/2 prevents MAPK pathway reactivation and combined with BRAFi, synergistically inhibits thyroid cancer growth[11].

The most common cause of thyroid cancer-related death is extrathyroidal invasion and metastasis[12]. While metastatic spread is less common in differentiated thyroid cancers[13], local invasion and distant metastasis occur often (~75%) in patients with undifferentiated thyroid cancer[14]. Notably, BRAF inhibitor resistance can also lead to a more aggressive metastatic phenotype in melanoma[15]. Understanding and preventing invasion and metastasis in PTC and ATC is therefore key to identifying effective treatment strategies. In this study, we focused on invasion, a key step in metastasis, and found that BRAFi paradoxically increases invasion in PTC and ATC cells resistant to BRAF inhibition. We therefore investigated a BRAF inhibitor-driven invasive phenotype as a mechanism of resistance in BRAF-V600E-mutated PTC and ATC. We identified a role for fibronectin (FN1) in an invasive phenotype, showed that invasion can be blocked with ERK1/2 inhibition, and identified EGR1 as a mechanism of fibronectin gene expression.

Materials and Methods

Reagents.

Dabrafenib (GSK2118436, BRAFi), vemurafenib (PLX4032), and SCH772984 (ERKi-SCH) were purchased from SelleckChem. Ulixertinib (ERKi-Uli) was purchased from MedChem Express. Fibronectin was purchased from Sigma. For *in vitro* studies, drugs were dissolved in either dimethyl sulfoxide (DMSO) for dabrafenib, vemurafenib, SCH772984,

and ulixertinib or water for fibronectin. For *in vivo* studies, dabrafenib and ulixertinib were dissolved in 1% carboxymethylcellulose.

Cell Culture.

Human thyroid cancer cell lines CUTC5 (RRID: CVCL_W916) and CUTC60 (RRID: CVCL_VM61) were generated in our laboratory in 2019[16]. BCPAP (RRID: CVCL_0153) and T238 (RRID: CVCL_6299) cells were kindly provided by Dr. M. Santoro and Dr. Roque, respectively, in 2007. Dr. J. Fagin provided the 8505C (RRID: CVCL_1054) and KTC1 (RRID: CVCL_6300) cell lines (with the permission of Dr. J. Kurebayashi for the KTC1 cell line) in 2007. BCPAP, KTC1, CUTC5, CUTC60, 8505C, and KTC1-VEMR human thyroid cancer cell lines were grown in RPMI (Invitrogen) supplemented with 5% FBS (HyClone Laboratories or Peak Serum). The T238 cell line was grown in RPMI supplemented with 10% FBS. The KTC1-VEMR (RRID: CVCL_A2CT) cell line, which acquired a *KRAS* G12D mutation as a mechanism of resistance[17], was developed by Dr. Marie-Claude Hofmann at MD Anderson Cancer Center in 2016. The KTC1-VEMR cell line was maintained in 1 μM vemurafenib. All cell lines were grown in 5% CO_2 at 37°C. Cell lines were monitored regularly for *Mycoplasma* using the Lonza Mycoalert system (Lonza Bioscience), validated using short tandem repeat profiling using the Applied Biosystems Identifier kit (#4322288) or Globalfiler® System (#4476135) at the Barbara Davis Center Molecular Biology Core Facility at the University of Colorado Anschutz Medical Campus, as previously described[18]. Authentication was last performed in 2019 for the CUTC5, KTC1, 8505C, T238, and KTC1-VEMR cell lines and 2021 for the BCPAP and CUTC60 cell lines after which all lines were batch frozen and not used beyond passage 20.

Matrigel-coated Boyden Chamber Invasion Assays.

Invasion assays were performed as described previously[19]. In brief, BRAF-V600E-mutated thyroid cancer cell lines were treated with indicated drug or corresponding vehicle and starved in RPMI with 0.1% FBS or conditioned media (CM) for 24 hrs. Cells were then plated in Matrigel-coated Boyden Chambers (Corning, chambers were either purchase pre-coated or were coated manually at a concentration of 300 μg/ml) with CM or media containing 0.1% FBS in the top chamber, media with 10% FBS as the chemoattractant in the bottom well, and indicated drug in both the top chamber and bottom well. An equal number of cells were plated in 6-well plates under identical conditions as each invasion chamber. After 24 hrs, cells that have invaded and adhered to the bottom of the Boyden Chambers were fixed with methanol, stained with DAPI, and counted using ImageJ, as described previously[19], or the Cytation 5 Cell Imaging Multi-Mode Reader (Agilent). For both imaging methods, nuclei were quantified at 10X magnification and ≥5 fields/invasion chamber. Cells from 6-well plates were lifted using Trypsin-EDTA (Gibco) and counted using the Vi-CELL XR Cell Viability Analyzer (Beckman Coulter). Cell counts were then used to normalize nuclei counts to cell growth.

Conditioned Media Collection.

The indicated BRAF-V600E-mutated thyroid cancer cell lines were plated in 15 cm dishes at a density that would result in 90% confluency after 72 hrs. After adhering overnight, cells were treated with the indicated drug or corresponding vehicle. 72 hrs later, media

containing drug was removed and plates were washed with 6 changes of PBS and replaced with RPMI media containing 1% FBS. After an additional 72 hrs, media from each plate was centrifuged at 1500 RPM for 5 min and filtered through a 0.45 μm pore, according to previous literature[20]. The cells from each plate were lifted using Trypsin-EDTA (Gibco) and counted using the Vi-CELL XR Cell Viability Analyzer (Beckman Coulter). Cell counts were then used to normalize ELISA data to cell growth.

Scratch-Wound Invasion Assays.

CUTC5 or CUTC60 cells were plated at a density of 40,000 or 20,000 cells/well, respectively, in 96-well IncuCyte® ImageLock plates. Cells were allowed to adhere overnight, followed by uniform wounding in all wells using a WoundMaker. Immediately after wounding, media was aspirated and each well was washed twice with PBS. PBS was aspirated and the indicated conditioned media supplemented with 4 mg/ml Matrigel was added to each well. Matrigel was allowed to polymerize at 37° C for 30 minutes. Images of each well were taken every 4 hrs for 72 hrs using the IncuCyte® ZOOM live-cell imaging system at 10X for subsequent analysis to measure percent wound confluence over time.

Revere Phase Protein Array.

Cells were treated with indicated compounds for 0, 4, or 72 hrs then harvested in RPPA lysis buffer (1% Triton X-100, 50 mM HEPES, pH 7.4, 150 mM NaCl, 1.5 mM MgCl2, 1 mM EGTA, 100 mM NaF, 10 mM Na pyrophosphate, 1 mM Na3VO4, 10% glycerol, protease and phosphatase inhibitor (Roche Applied Science) and diluted in SDS Sample Buffer (40% Glycerol, 8% SDS, 0.25M Tris-HCL, pH 6.8). Before use, β-mercaptoethanol at 1/10 of the volume was added. RPPA was performed by the MD Anderson Cancer Center Functional Proteomics RPPA Core Facility for 304 unique antibodies, which were analyzed on Array-Pro then by SuperCurve Rx64 3.1.1. Protein levels were then determined by interpolation of dilution curves to give Log2 values. The data was then normalized for protein loading and transformed to linear values. Fold-change values were calculated using multiple-comparisons ANOVA.

Western Blotting.

Performed as described previously[11]. In brief, cells were treated with the indicated compounds and harvested in CHAPS lysis buffer (10 mM CHAPS, 50 mM Tris (pH 8.0), 150 nM NaCl, and 2 mM EDTA) with phosphatase and protease inhibitor cocktail (Roche). Protein lysates were resolved on SDS-PAGE gels, transferred to Immobilon-FL membranes (Millipore), then incubated at 4°C overnight with the indicated antibodies diluted in 1:3 Intercept Blocking Buffer in TBST (LICOR) or 5% BSA in TBST. Antibodies used in western blot experiments: α-tubulin, β-actin, EGR1, pT202Y204 ERK1/2, ERK1/2, fibronectin, vinculin (RRID:AB_2617116, RRID:AB_2242334, RRID:AB_2616601, RRID:AB_10695739, RRID:AB_2315112, RRID:AB_2924220, RRID:AB_2728768). Blots were incubated with secondary goat anti-mouse or anti-rabbit IRDye-conjugated antibodies (LICOR) and proteins were imaged and quantified with the Odyssey CLx imager (Image Studio Acquisition Software Version 5.2.5, LICOR).

Fibronectin ELISA Assays.

To measure fibronectin secretion, CM was collected as described above[20], and subject to the Fibronectin Human ELISA Kit (Invitrogen, BMS2028 or Abcam, ab219046). To compare human (tumor-derived) vs mouse (stroma-derived) fibronectin *in vivo*, blood was collected from mice at the end of study using cardiac puncture following cervical dislocation. Whole blood was placed in tubes with 8 μl of EDTA then centrifuged at 1,500 RCF for 10 min. Plasma was transferred to clean tubes. Human and mouse fibronectin was measured using the Human Fibronectin ELISA kit (Abcam, ab219046) or Mouse Fibronectin ELISA kit (Abcam, ab210967) according to the manufacturer protocols.

Affymetrix Array.

Gene expression data was generated previously using Affymetrix Human Genome U133 Plus 2.0 microarrays[18]. Briefly, quality control was performed using the arrayQualityMetrics package from Bioconductor 3.5 in R, Affymetrix Power Tools was used to perform background subtraction and quantile normalization, and probe sets were collapsed to genes using GSEA v2.1.0 software.

Fibronectin and EGR1 shRNA Knockdown.

For fibronectin (FN1) knockdown, lentivirus was generated using MISSION® shRNA clones TRCN0000293839 (shFN1–1), TRCN0000286357 (shFN1–2), and SHC216 (shScr) using a previously established protocol[19]. In brief, to HEK293FT cells, expression vector, packaging vector 1, packaging vector 2, SHC216 (scramble) plasmid, TRCN0000293839 (shFN1–1) plasmid, TRCN0000286357 (shFN1–2) plasmid, Enhancer (Qiagen), and Effectene (Qiagen) were added. Lentivirus was collected after 48 and 72 hrs then added to BRAF inhibitor resistant CUTC60 cells with Polybrene (Sigma). Transduced cells were selected with Puromycin (Sigma). shEGR1 (early growth response 1) knockdown cells were generated as described above using MISSION® shRNA clones TRCN0000273910 (shEGR1–1), TRCN0000273850 (shEGR1–2), and SHC216 (shScr).

CellTiter-Glo 2.0 Assay.

Cells (1500/well for CUTC5, 1000/well for CUTC60 parental, shScr, shFN1–1, and shFN1–2) were plated in triplicate in white-walled 96-well plates and treated with increasing concentrations of indicated drugs for 72 hrs. Cell growth was measured with CellTiter-Glo 2.0 reagent (Promega) using the manufacturer's protocol. Luminescence was read using the Biotek Synergy H1 plate reader and cell viability was calculated by the intensity of luminescence in relation to vehicle-treated wells.

ViCell Growth Assay.

Parental CUTC60, shScr, shFN1–1, or shFN1–2 cells were plated in duplicate in 6-well plates. After 7 days, cells were lifted from the plates using Trypsin-EDTA, and cell count was determined using the Vi-CELL XR Cell Viability Analyzer (Beckman Coulter).

Immunohistochemistry and Pathologist Scoring.

Immunohistochemistry (IHC) staining for fibronectin was performed and scored as percent positive cells by a blinded pathologist. Antibody used for IHC: fibronectin/ RRID:AB_2924220. For fibronectin, slides were baked for 1 hr at 60°C, deparaffinized in 2 changes of xylene, rehydrated through ethanols from 100% to 80%, then rinsed 3 times in deionized water. Antibody retrieval was performed for 15 min at 110°C in Citrate Buffer (2.1g citric acid monohydrate, 1L deionized water, 0.5 ml Tween 20, pH 6). Slides were then rinsed in wash buffer (PBS/0.1% Tween 20), blocked for 10 min in 3% H_2O_2, blocked with normal goat serum for 1 hr, then incubated with primary antibody at 4°C for 24 hrs. Goat anti-rabbit polymer was added for 30 min followed by DAB chromogen (Vector Labs). Slides were counterstained with Hematoxylin (Vector Labs), rinsed in water, differentiated in 1% NaOH, then dehydrated from 95% to 100% ethanol. Coverslips were applied after 4 changes of xylene.

Patient-Derived Xenograft Model.

All animal experiments were performed under an approved University of Colorado Anschutz Medical Campus Institutional Animal Care and Use Committee (IACUC) protocol. Six control mice and six experimental mice were needed per group to allow for two tumors per mouse, for a total of 12 tumors per group. Based on previous data[16], this allows for sufficient power (0.8) to detect at least a 50% difference between groups. CUTC60-PDX tumors, developed previously in our lab[16] were chopped into 3 mm pieces and submerged in Cultrex BME Type 3 (Bio-Techne). Female athymic nude-Foxn1nu mice (Envigo) were anesthetized with isoflurane and the CUTC60-PDX tumor chunks were inserted via trocar injection into the left and right flanks. Tumor establishment and progression was monitored through caliper measurement. Tumor volume was calculated by (W^2 x L)/2 (W: Width, L: Length). Once tumors reached an average of 100 mm^3, mice were randomized to receive vehicle, BRAFi (30 mg/kg), ERKi-Uli (50 mg/kg), or the combination, each in 100 ul of 1% carboxymelthycellulose. After day 55, BRAFi was increased to 50 mg/kg and ERKi-Uli was increased 100 mg/kg for the single-agent and combination treatment groups. At study end, mice were anesthetized using isoflurane and euthanized via cervical dislocation followed by exsanguination by cardiac puncture. Final tumor volumes were calculated by (length x width x height)*0.5236.

RNA-Sequencing.

CUTC60 cells were plated in 10 cm dishes, allowed to adhere for 24 hrs, then treated with either BRAFi (100 nM), ERKi-Uli (1 μM), or the combination. After 48 hrs, RNA was isolated from each plate using an RNeasy Kit (Qiagen). RNA-sequencing was performed through the University of Colorado Cancer Center Shared Genomics Core using the Universal Plus™ library preparation kit. Paired-end 150 bp-long sequences were aligned to the hg38 human reference genome using STAR RNA-seq aligner[21]. Transcript counts were estimated with the help of htseq-count script from HTSeq 0.11.1[22] (GEO accession number: GSE221329).

Quantitative PCR (qPCR).

RNA was isolated using the RNeasy Kit (Qiagen). qPCR was performed in the PCR Core Facility in the Division of Endocrinology, Metabolism and Diabetes at the University of Colorado Anschutz Medical Campus.

Statistical Analysis.

An independent t-test was used for comparing means of two groups and one-way analysis of variance (ANOVA) was used to compare means of more than two groups. Signal analysis via Odyssey CLx imager (LICOR) was used for quantification of western blots. Following alignment by a bioinformatician, RNA-sequencing data was analyzed using BioJupies[23]. Data represented as means ± SEM. *, $P < 0.05$; **, $P < 0.01$; ***, $P < 0.001$; ****, $P < 0.0001$, ns = not significant.

Data Availability.

The data generated in this study are available upon request.

Results

BRAFi-resistant cell lines exhibit a pro-invasive phenotype and secretome in response to BRAF inhibition.

Five-year survival rates of patients with distant metastatic thyroid cancer are significantly worse (~53%) than patients with localized or regional thyroid cancer (~98%)[24]. Furthermore, mutations in BRAF-V600E have been associated with more aggressive clinicopathological features, including extrathyroidal invasion[25]. Invasion is a critical step in the metastatic cascade and has been associated with resistance to therapy[26,27]. We therefore hypothesized that an invasive phenotype plays a role in sensitivity versus resistance to BRAF-directed therapy. To test this hypothesis, we evaluated invasion using Matrigel-coated Boyden Chamber invasion assays in response to the BRAF inhibitor, dabrafenib (BRAFi), in a panel of BRAF-V600E-mutated cell lines. We previously calculated area under the dose-response curve (AUC) values for this panel of cell lines to determine their sensitivity or resistance to MAPK-pathway inhibitors, and the effects of BRAF and ERK1/2 inhibition on MAPK pathway activation in thyroid cancer[11]. Table 1S shows the cell lines used herein and their sensitivity to BRAFi. This panel includes cell lines that are BRAFi-sensitive (KTC1, CUTC5; AUC > 0.7), moderately resistant to BRAFi (8505C; AUC 0.4 – 0.7), strongly resistant to BRAFi (T238, CUTC60; AUC < 0.3), or have acquired resistance to BRAFi (KTC1-VEMR) due to acquisition of a KRAS G12R mutation[17]. Interestingly, treatment with clinically relevant concentrations of BRAFi (100 nM) increases invasion 1.7 to 2.6-fold in cells with intrinsic or acquired resistance, but not in cells that are sensitive to BRAFi (Figure 1A, $p < 0.009$). To determine whether BRAFi also promotes cell migration in resistant cells, we treated four BRAFi-resistant cell lines with BRAFi (100 nM) and measured migration through uncoated Boyden Chambers. Interestingly, we only identified an increase in cell migration in response to BRAFi in one cell line (T238, Figure S1A), and therefore chose to focus on cell invasion.

To determine whether baseline invasiveness differs between sensitive and resistant cell lines, we compared invasion of each untreated cell line. Figure S1B shows that baseline invasion normalized to cell growth of each cell line does not significantly differ between cell lines that are sensitive or resistant to BRAF inhibition. Together, these data show that BRAF-V600E-mutated thyroid cancer cell lines resistant to BRAF inhibition exhibit increased invasion in response to BRAFi treatment. This aligns with previous studies that demonstrate an invasive phenotype in response to BRAF inhibition in *BRAF*-mutant melanoma as a mechanism of drug resistance[27].

Extracellular molecules play a crucial role in mediating signal transduction and thereby controlling cancer cell invasion[28]. We hypothesized that BRAF inhibition could promote secretion of pro-invasive factors, leading to increased invasion. To determine whether secreted factors promote invasion in response to BRAFi, we collected conditioned media (CM) from cells sensitive or resistant to BRAFi. Using Matrigel-coated Boyden Chamber invasion assays, we show 24 hrs of treatment with CM from sensitive CUTC5 or KTC1 cells treated with BRAFi does not increase the invasiveness of sensitive CUTC5 cells nor resistant CUTC60 cells (Figure 1B, Figure S1C). However, CM from cells with intrinsic (CUTC60) or acquired (KTC1-VEM) resistance promotes invasion in both sensitive CUTC5 (2.6 to 3.0-fold, $p < 0.007$ Figure 1B, Figure S1C) and resistant CUTC60 cells (2.4 to 3.0-fold, $p < 0.01$ Figure 1B, Figure S1C). To confirm this finding, we performed Scratch-Wound invasion assays to measure invasion of CUTC5 and CUTC60 cells through Matrigel supplemented with CM from vehicle or BRAFi-pretreated CUTC60 cells. Percent wound confluence was measured over 72 hrs, then AUC analysis was used to quantify the results. In Figure 1C, we show that CM from resistant CUTC60 cells treated with BRAFi increases wound closure through Matrigel of both sensitive CUTC5 and resistant CUTC60 cells. Percent wound confluence over 72 hrs and representative images of Figure 1C are shown in Figure S1C and E, respectively.

BRAF inhibition increases cellular and secreted fibronectin, which promotes invasion.

To identify mediators of an invasive phenotype in response to BRAF inhibitor treatment, we treated the BRAF-V600E-mutant ATC cell line 8505C with the BRAF inhibitor vemurafenib for 0, 4, or 72 hrs. We then screened a panel of >300 proteins and phosphoproteins using the MD Anderson Cancer Center Reverse Phase Protein Array (RPPA) platform (Table S2). We calculated fold change for each protein in response to treatment along with multiple comparisons ANOVA to compare treatment groups. Of the top 20 regulated proteins, 12 are upregulated in response to BRAF inhibitor treatment and 8 are downregulated (Figure 2A). Of those, we focused on FN1 (fibronectin), which is a secreted glycoprotein that promotes invasion and is regulated by the MAP kinase pathway[29]. Furthermore, high fibronectin expression levels have been associated with *BRAF*-mutant thyroid tumors[30]. We further determined the correlation of fibronectin expression with relapse-free survival using Kaplan-Meier analysis of 502 thyroid carcinoma patient samples[31], which indicates that higher fibronectin expression is correlated with a lower relapse-free survival in thyroid cancer (KM-plotter; $p = 7\times10^{-5}$).

To determine the role of fibronectin in BRAFi resistance, we first confirmed the upregulation of fibronectin observed via RPPA in additional cell lines using western blotting, which show a 1.9 to 5.1-fold increase in fibronectin in response to BRAFi in sensitive and resistant cells (Figure S2A). Increased fibronectin expression in response to BRAFi also correlates with an increase or rebound of pERK1/2, which we have previously described[11]. To characterize the effects of BRAFi treatment on fibronectin secretion, we performed ELISA assays on CM and found that fibronectin secretion increases by 1.8 to 3.0-fold in response to BRAFi in resistant cell lines but decreases or remains that same in sensitive cell lines (Figure 2B). Figure S2B shows levels of secreted fibronectin non-normalized to cell number or vehicle-treated cells. These data suggest that fibronectin secretion increases in response to BRAFi in resistant cells, supporting our findings in Figure 1B, which demonstrate an increase in secreted factors promote invasion in response to BRAF inhibition.

Based on these data, we next sought to determine whether addition of fibronectin is sufficient to increase invasion of BRAFi-resistant cells. We performed Matrigel-coated Boyden Chamber invasion assays in media supplemented with fibronectin to mimic levels comparable to those observed via ELISA (100 ng/ml). Figure 2C shows that treatment with fibronectin phenocopies BRAFi treatment by increasing invasion 1.7 to 2.6-fold in two BRAF-V600E-mutated resistant cell lines.

To quantifiably compare baseline levels of fibronectin protein and transcript in sensitive and resistant cells, we analyzed our RPPA data and previously published Affymetrix microarrays[18] on our panel of 16 BRAF-V600E-mutated thyroid cancer cell lines. While cells resistant to BRAFi have lower levels of fibronectin protein, this trend is not significant (Figure S3A). This remains the case when comparing cell lines based on their dependency on the MAPK-pathway for growth, where cell lines independent of MAPK signaling have an AUC of <0.5 for both MEK1/2 inhibition (trametinib) and ERK1/2 inhibition (SCH772984, ERKi-SCH), as previously established in our laboratory[11] (Figure S3A). Accordingly, Affymetrix data shows no significant difference between fibronectin transcript levels in sensitive or resistant cells (Figure S3B).

Fibronectin is necessary for a BRAFi-induced invasive phenotype.

To determine whether fibronectin depletion regulates cell growth in response to BRAF inhibition, we knocked down fibronectin using two unique, validated shRNAs, along with a scramble control (shScr) and generated stable control or fibronectin-depleted cell lines derived from the BRAFi-resistant CUTC60 cell line (Figure 3A, ≥ 80% knockdown). We performed CellTiter-Glo 2.0 assays using the parental CUTC60 cells, shScr cells, and fibronectin knockdown cell lines. We found that cells with depleted fibronectin remain resistant to BRAF inhibition (Figure S4A), which was confirmed by ViCell counting over 7 days (Figure S4B), together indicating that fibronectin does not regulate cell growth in response to BRAF inhibition.

To determine the necessity of fibronectin for a BRAFi-induced invasive phenotype, we used fibronectin ELISA assays to show that parental CUTC60 cells exhibit a 2.5 to 2.7-fold increase in fibronectin secretion in response to BRAFi ($p < 0.0001$), similar to the shScr

control cells (3.6 to 3.8-fold). Consistent with our hypothesis, the shFN expressing cells fail to induce fibronectin secretion (Figure 3B) and fail to exhibit a BRAFi-induced increase in invasion (Figure 3C, Figure S4C). These data demonstrate that fibronectin expression is necessary for a BRAFi-induced invasive phenotype.

To specifically determine the role of secreted fibronectin, we collected CM from shFN1–1 and shFN1–2 CUTC60 knockdown cells and performed Boyden chamber invasion assays as in Figure 1B. CM from BRAFi-treated fibronectin-depleted cell lines does not increase invasion to the same extent as CM from BRAFi-treated cells with endogenous levels of fibronectin (Figure 3D), suggesting fibronectin contributes to a pro-invasive secretome. Representative images of the data in Figure 3D are shown in Figure S4D.

Effects of fibronectin depletion on phoshpo-ERK1/2 and fibronectin.

To characterize how fibronectin depletion impacts MAPK-signaling in response to BRAF inhibition, we performed western blots for fibronectin, ERK1/2, and pERK1/2 in the CUTC60 fibronectin knockdown cell lines (Figure S4E). Quantification of protein levels show that in parental, scramble control, and fibronectin knockdown cell lines, pERK1/2 is initially inhibited at 48 hrs, but rebounds by 72 hrs. We further found that while fibronectin is initially increased at 48 hrs in response to BRAFi treatment in all cell lines, parental and scramble control cells sustain increased fibronectin levels while the fibronectin-depleted cell lines do not (Figure S4E). These data show that in the fibronectin-knockdown cell lines, fibronectin remains depleted in response to BRAFi treatment and that loss of fibronectin does not affect pERK1/2.

ERK1/2 inhibition can block an invasive phenotype in BRAFi-resistant cell lines.

We next sought to inhibit the BRAFi-driven invasive phenotype. The most common mechanism of resistance to inhibition of the MAPK-pathway is pathway reactivation[32,33]. Indeed, we have previously shown that in response to single agent BRAFi, pERK1/2 rebound occurs in 48–72 hrs, which is blocked by combined BRAF and ERK1/2 inhibition[11]. To further understand the importance of ERK1/2 signaling in thyroid cancer, we correlated ERK Score[34] with thyroid cancer clinical outcomes, including Tumor Stage (according to the American Joint Committee on Cancer Tumor Stage Code) and Risk Group (as described by the American Thyroid Association (ATA)) in >1,600 thyroid cancer patient samples in cBioPortal. This analysis revealed that patients with a higher Tumor Stage (T3) have significantly higher ERK Scores compared with patients with a low Tumor Stage (T1) (Figure S5). Additionally, patients with an intermediate to high risk of recurrence exhibit higher ERK Scores than patients with a low risk of recurrence (Figure S5). These results indicate that ERK Score may be a valuable indicator of thyroid tumor staging and ATA risk of recurrence.

Because fibronectin expression can be regulated by MAPK signaling and MAPK signaling is associated with higher risk of recurrence and tumor stage, we hypothesized that preventing MAPK-pathway reactivation through combined BRAF/ERK1/2 inhibition would ablate the BRAFi-induced invasive phenotype. Using ELISA assays, we found that BRAFi induces a 1.7 to 2.1-fold increase in secreted fibronectin in the CUTC60 and 8505C cells,

as shown above ($p < 0.005$, Figure 4A). Interesting, ERKi with SCH772984 alone decreases or does not affect baseline fibronectin secretion, but reduces the induction of fibronectin secretion by dabrafenib (Figure 4A, $p < 0.007$, CUTC60).

Given that fibronectin secretion is reduced by BRAF and/or ERK1/2 inhibition, we next tested whether inhibition of BRAF or ERK1/2 could overcome fibronectin-induced invasion. In Figure 4B, we compared invasiveness of cells treated with ERKi-SCH alone to treatment with combinations of BRAFi, ERKi-SCH, and fibronectin. We show that combined BRAFi and fibronectin treatment increases invasion 2.6–fold in the CUTC60 cells ($p = 0.03$) and, while variable, 2.8-fold in the 8505C cells. In both CUTC60 and 8505C cells, ERK1/2 inhibition overcomes BRAFi-induced and fibronectin-induced invasion in resistant cell lines, as indicated by the lack of increased invasion in CUTC60 or 8505C cells treated with combined ERKi and fibronectin or combined ERKi and BRAFi. These data indicate that ERK1/2 inhibition can prevent an invasive phenotype, characterized by fibronectin secretion and increased invasion.

Combined BRAF and ERK1/2 inhibition reduces tumor growth and fibronectin in vivo.

We next hypothesized that BRAF and ERK1/2 inhibition would reduce tumor growth and fibronectin *in vivo.* For these studies, we used a BRAF-V600E-mutant patient-derived xenograft (PDX) model of ATC (CUTC60-PDX)[16] to best recapitulate the human tumor microenvironment. Further, the CUTC60-PDX was derived from the same patient as the CUTC60 cell line used *in vitro.* For this animal model, we used the ERK1/2 inhibitor ulixertinib (ERKi-Uli), as it is farthest along in clinical trials[35]and confirmed that ERKi-SCH and ERKi-Uli have similar effects on cell growth, in representative sensitive (CUTC5) and resistant (CUTC60) cell lines (Figure S6).

For these studies, we injected BRAFi-resistant CUTC60-PDX tumor chunks into the flanks of athymic nude mice, allowed the tumors to reach an average of $100mm^3$, randomized mice into four groups, then began treatment with vehicle, BRAFi (30 mg/kg), ERKi-Uli (50 mg/kg), or the combination via daily oral gavage (Figure 5). After 30 days of treatment (55 days following tumor implantation), drug doses of BRAFi and ERKi-Uli were increased to 50 mg/kg and 100 mg/kg daily. Tumor volume was calculated via biweekly caliper measurements and mice were weighed weekly. Combination BRAFi and ERKi-Uli treatment slowed tumor growth, and mice in the combination group had smaller tumors than those in the vehicle-treated group at the end of study (Figure 5A). Mice in all treatment groups gained weight steadily throughout the experiment, suggesting little to no toxicity associated with drug treatment (Figure 5B), as described in other tumor types[35]. Of note, histologic analysis revealed no significant changes in invasion (Figure S7) and no metastatic spread to the lungs, likely due to the rapid growth of the CUTC60-PDX.

To determine the role of fibronectin *in vivo*, peripheral blood was harvested at the time of sacrifice, plasma was isolated, and mouse- and human-specific fibronectin ELISA to measure stroma-derived and tumor-derived circulating fibronectin, respectively, were performed. In Figure 5C, we show that stroma-derived and tumor-derived circulating fibronectin levels are moderately increased in mice treated with BRAFi and are decreased 1.4 to 1.7-fold in mice treated with combined BRAFi and ERKi-Uli (stroma-derived: p =

0.11; tumor-derived: p = 0.02). This shows combined BRAF/ERK1/2 inhibition can reduce circulating fibronectin levels *in vivo.* We next assessed fibronectin levels in the tumors by histologic analysis, and while not significant, we observed a 1.6-fold increase in tumoral fibronectin in mice treated with BRAFi compared to vehicle-treated mice (Figure 5D). Treatment with ERKi-Uli did not affect percent fibronectin staining in the tumors compared to vehicle treatment. Together, the regulation of secreted fibronectin *in vivo* correlates well with our *in vitro* observations (Figure 4A).

Combined BRAF and ERK1/2 inhibition decreases EGR1 levels and transcriptional targets.

We next focused on signaling proteins downstream of fibronectin that could mediate increased invasion. We found transcript levels of integrin pair $\alpha_5\beta_1$, the primary receptor for fibronectin that is responsible for cell invasion[36], do not differ between sensitive and resistant cell lines (Figure S3C). Expression and phosphorylation of downstream signaling components MET, FAK (PTK2), or SRC also do not differ between sensitive and resistant cells (Figure S3D–I).

Reprogramming of the transcriptome has been associated with tumor plasticity and an invasive phenotype. We therefore used RNA-sequencing to characterize gene expression changes that occur in response to BRAF and ERK1/2 inhibition in *BRAF*-mutated thyroid cancer cells. We treated resistant (CUTC60) cells with vehicle, BRAFi, ERKi-Uli, or the combination for 48 hrs, isolated RNA, then performed RNA-sequencing through the University of Colorado Cancer Center Shared Genomics Core. Figure 6A shows a volcano plot generated using Biojupies[23] comparing BRAFi-treated to combined BRAFi/ERKi-Uli-treated resistant CUTC60 cells. The most differentially regulated gene between these groups is the transcription factor Early Growth Response 1 (*EGR1*), which is known to be regulated by ERK1/2[37]. We confirmed these RNA-seq results using western blots to show that BRAF inhibitor treatment increases EGR1 in resistant CUTC60 cells, while ERKi-Uli decreases EGR1 (Figure 6B). Similar results were observed in additional resistant cell lines (Figure S8A). Comparatively, in sensitive CUTC5 cells, treatment with BRAFi, ERKi-Uli, or the combination decreases EGR1 expression (Figure 6B). We further performed ChIP Enrichment Analysis and as shown in Figure 6A, *EGR1* target genes are also down-regulated in the combination-treated cells compared to BRAFi-treated resistant CUTC60 cells. Of interest, the promoter of fibronectin contains two EGR1 consensus sites, and it has been shown that EGR1 can promote increased fibronectin and cell attachment[37].

To determine whether *EGR1* regulates BRAFi-induced invasion, we generated EGR1 knockdown cell lines using two distinct shRNAs in BRAFi-resistant CUTC60 cells, alongside a shScr control (Figure 6C). As shown above, BRAFi increases invasion in parental and ShScr cell lines by ~2-fold. However, BRAFi treatment does not increase invasion in cells with depleted EGR1, suggesting EGR1 is necessary for a BRAFi-induced invasive phenotype (Figure 6D). Finally, we asked whether EGR1 is necessary for a BRAFi-induced increase in fibronectin, which is a known target of EGR1[37,38]. We performed western blots to show that in cells with depleted EGR1, BRAFi does not increase cellular fibronectin to the same extent as in cells with endogenous levels of EGR1 (Figure 6E). To determine the regulation of fibronectin gene expression by EGR1, we treated parental,

shScr, or shEGR1 knockdown cell lines with BRAFi for 48 hrs, and measured fibronectin expression by qPCR. Figure 6F shows that induction of fibronectin in response to BRAFi is reduced in shEGR1 expressing cells compared to parental or shScr-expressing cells. Together these data indicate that ERK1/2 inhibition prevents an invasive phenotype through regulation of EGR1, which limits fibronectin induction (Figure 6).

Discussion

Advanced thyroid cancer has few effective, targeted therapeutic options. While *BRAF* mutations are common and targetable in advanced thyroid cancer, many patients exhibit intrinsic or acquired resistance over time[5], which can lead to a more aggressive metastatic phenotype[15]. Further, the most common cause of thyroid cancer-related death is extrathyroidal invasion and metastasis[12], which occurs in ~75% of patients with undifferentiated thyroid cancer[14]. The paradox of BRAF inhibitors, primarily vemurafenib, increasing invasion has been previously observed in *BRAF*-mutant cancers[26,27] and therefore, goes beyond our findings reported here in *BRAF*-mutant thyroid cancer. Thus, deciphering mechanisms of thyroid cancer invasion in response to therapy is vital to improving patient outcomes.

In this study, we focused on the role of an invasive phenotype in mediating resistance to BRAF inhibition. Figure 7 depicts a model in which BRAF inhibition drives an invasive phenotype in advanced thyroid cancer. In this study, we found that the BRAF inhibitor dabrafenib promotes invasion and a pro-invasive secretome (Figure 1) through the induction of cellular and secreted fibronectin (Figure 2–3). Fibronectin is an ECM protein that regulates cell adhesion, migration, and invasion[39]. Fibronectin matrices act as linkers between ECM to facilitate signal transduction and have been shown to regulate FAK/SRC, PI3K/AKT, and MAPK signaling. Upon analyzing potential mediators of an invasive phenotype through fibronectin, we identified no differences in fibronectin and $\alpha_5\beta_1$ integrin expression or activation of MET, FAK, or SRC between cells that are sensitive or resistant to BRAFi. These results suggest that baseline levels of signaling molecules do not correlate significantly with sensitivity to BRAF inhibition. Instead, we found that an increase in fibronectin expression in response to BRAFi-treatment is indicative of a pro-invasive phenotype. This corroborates the data shown in Figure S1B, which demonstrates no significant difference in invasion between sensitive and resistant cell lines at baseline, rather, an in increase in invasion is only observed in response to BRAFi treatment (Figure 1A).

In melanoma, it has been shown that BRAF inhibition is associated with increases in fibronectin-mediated adhesion signaling[40] and that fibronectin promotes invasion, adaptive plasticity, and BRAF inhibitor resistance[41]. Secretion of fibronectin has also been shown to promote metastasis in ovarian cancer[42]. Further, fibronectin expression is higher in *BRAF*-mutant thyroid tumors[43], and our Kaplan-Meier Plotter analysis indicates fibronectin expression is correlated with a lower relapse-free survival in thyroid cancer (KM-plotter; $p = 7\times10^{-5}$)[31], and predicts the presence of lymph node metastases[44], providing key clinical relevance to the role of fibronectin in invasion and metastasis of advanced thyroid cancer. Thus, future studies are needed to specifically evaluate the role of BRAFi-induced fibronectin in thyroid cancer metastasis.

To block a BRAF inhibitor-induced invasive phenotype, we inhibited BRAF and ERK1/2 and show this combination can prevent invasion *in vitro*, slow tumor growth, and decrease circulating fibronectin *in vivo.* To understand the mechanism of BRAFi-induced invasion, we characterized gene expression differences between BRAFi-treated cells and combined BRAFi/ERKi-Uli-treated cells. This analysis identified down-regulation of the transcription factor EGR1 as a potential mechanism by which combined BRAF/ERK1/2 inhibition prevents an invasive phenotype. Previous studies have shown that EGR1 upregulates fibronectin gene expression through two EGR1 binding sites in the proximal fibronectin promoter[37,38]. While ERK1/2 does not directly regulate EGR1, ERK1/2 phosphorylates ELK1 to upregulate its transcriptional activity[45]. ELK1 has been shown to transcriptionally upregulate EGR1 via binding to serum response element sites on the *EGR1* promoter[45]. Thus, ERK1/2 regulation of ELK1 is a potential mechanism by which ERK1/2 regulates EGR1 and ultimately fibronectin (Figure 7).

Invasive phenotype switching has been most extensively studied in melanoma, where low levels of MITF and high WNT5A have been shown to promote invasion[46]. Accordingly, studies have shown that inhibition of WNT5A can inhibit invasion[46]. However, fibronectin, E-cadherin, and other ECM proteins as well as transcription factors involved in epithelial-to-mesenchymal transition (EMT) have also been shown to contribute to the invasive phenotype[47]. These results demonstrate how multifaceted an invasive phenotype is in therapy resistance. Therefore, inhibition of an ERK1/2/EGR1/Fibronectin axis likely represents one of many potential strategies to prevent an invasive phenotype as a mechanism of resistance to MAPK-directed therapies in thyroid cancer.

There is mounting clinical interest in targeting the ECM as a potential treatment strategy for cancer patients. Fibronectin is a prominent component of normal and tumoral microenvironments, composed of type I, type II, and type III domains[48]. In the context of development and cancer, splice isoforms containing the type III domains EDA and EDB (Extra Domains A and B, or EIIIA and EIIIB), referred to as oncofetal or embryonic fibronectin, are commonly expressed[48]. Recently, nanobodies have been developed that specifically target and inhibit embryonic fibronectin[49] and peptide drugs that target fibronectin are currently in development[50]. In light of these advances, future studies will explore the role of the ERK1/2/EGR1/Fibronectin axis in metastasis and inhibition of tumoral fibronectin as a method to prevent invasion and ultimately metastasis in advanced thyroid cancer.

Supplementary Material

Refer to Web version on PubMed Central for supplementary material.

Acknowledgements:

This research was supported by the National Institutes of Health National Cancer Institute (NIH NCI F31 Grant # 1F31CA257079 to H.M. Hicks; NIH NCI R01 Grant # 1R01CA222299 and 1R01CA164193 to R.E. Schweppe). The authors acknowledge support from the MD Anderson Cancer Center Functional Proteomics RPPA Core Facility supported by NCI Grant # CA16672 and NIH R50 Grant # R50CA221675 (Yiling Lu), the University of Colorado Cancer Center Genomics Shared Resource supported by P30CA046934, and Sarah Hartman in the laboratory of Dr. Todd Pitts for training on trocar injections for tumor implantation in our patient-derived xenograft

animal model. We also thank Dr. Christopher Korch for cell line authentication advice. We finally thank Meghan Kellett and Dr. Madison Rose for technical support and input on experimental design, and Dr. Bryan Haugen for critical reading of our manuscript.

References:

1. Tavares C. et al. NIS expression in thyroid tumors, relation with prognosis clinicopathological and molecular features. Endocr Connect 7, 78–90 (2018). 10.1001/jamaoncol.2020.3362 [PubMed: 29298843]
2. Maniakas A. et al. Evaluation of Overall Survival in Patients With Anaplastic Thyroid Carcinoma, 2000–2019. JAMA Oncol 6, 1397–1404 (2020). 10.1001/jamaoncol.2020.3362 [PubMed: 32761153]
3. Xing M. Molecular pathogenesis and mechanisms of thyroid cancer. Nat Rev Cancer 13, 184–199 (2013). 10.1038/nrc3431 [PubMed: 23429735]
4. Poulikakos PI, Sullivan RJ & Yaeger R. Molecular Pathways and Mechanisms of BRAF in Cancer Therapy. Clin Cancer Res (2022). 10.1158/1078-0432.CCR-21-2138
5. Crispo F. et al. BRAF Inhibitors in Thyroid Cancer: Clinical Impact, Mechanisms of Resistance and Future Perspectives. Cancers (Basel) 11 (2019). 10.3390/cancers11091388
6. Subbiah V. et al. Dabrafenib and Trametinib Treatment in Patients With Locally Advanced or Metastatic BRAF V600-Mutant Anaplastic Thyroid Cancer. J Clin Oncol 36, 7–13 (2018). 10.1200/JCO.2017.73.6785 [PubMed: 29072975]
7. Porter A. & Wong DJ Perspectives on the Treatment of Advanced Thyroid Cancer: Approved Therapies, Resistance Mechanisms, and Future Directions. Front Oncol 10, 592202 (2020). 10.3389/fonc.2020.592202 [PubMed: 33569345]
8. Subbiah V, Baik C. & Kirkwood JM Clinical Development of BRAF plus MEK Inhibitor Combinations. Trends Cancer 6, 797–810 (2020). 10.1016/j.trecan.2020.05.009 [PubMed: 32540454]
9. Kulkarni P, Hall J, Wang L. & Henderson S. Papillary Thyroid Cancer Differentiating Into Anaplastic Carcinoma With Near-Complete Response to Targeted Dabrafenib/Trametinib Combination Therapy. Cureus 13, e20693 (2021). 10.7759/cureus.20693 [PubMed: 35106230]
10. Morris EJ et al. Discovery of a Novel ERK Inhibitor with Activity in Models of Acquired Resistance to BRAF and MEK Inhibitors. Cancer Discovery 3, 742–750 (2013). 10.1158/2159-8290.Cd-13-0070 [PubMed: 23614898]
11. Hicks HM et al. Inhibition of BRAF and ERK1/2 has synergistic effects on thyroid cancer growth in vitro and in vivo. Mol Carcinog 60, 201–212 (2021). 10.1002/mc.23284 [PubMed: 33595872]
12. Banerjee M, Muenz DG, Chang JT, Papaleontiou M. & Haymart MR Tree-based model for thyroid cancer prognostication. J Clin Endocrinol Metab 99, 3737–3745 (2014). 10.1210/jc.2014-2197 [PubMed: 25033070]
13. Ruegemer JJ et al. Distant metastases in differentiated thyroid carcinoma: a multivariate analysis of prognostic variables. J Clin Endocrinol Metab 67, 501–508 (1988). 10.1210/jcem-67-3-501 [PubMed: 3410936]
14. Limaiem F, Kashyap S, Naing PT & Giwa AO in StatPearls (2022).
15. Emmons MF, Faiao-Flores F. & Smalley KSM The role of phenotypic plasticity in the escape of cancer cells from targeted therapy. Biochem Pharmacol 122, 1–9 (2016). 10.1016/j.bcp.2016.06.014 [PubMed: 27349985]
16. Schweppe RE et al. Establishment and Characterization of Four Novel Thyroid Cancer Cell Lines and PDX Models Expressing the RET/PTC1 Rearrangement, BRAFV600E, or RASQ61R as Drivers. Mol Cancer Res 17, 1036–1048 (2019). 10.1158/1541-7786.MCR-18-1026 [PubMed: 30733375]
17. Danysh BP et al. Long-term vemurafenib treatment drives inhibitor resistance through a spontaneous KRAS G12D mutation in a BRAF V600E papillary thyroid carcinoma model. Oncotarget 7, 30907–30923 (2016). 10.18632/oncotarget.9023 [PubMed: 27127178]

18. Landa I. et al. Comprehensive Genetic Characterization of Human Thyroid Cancer Cell Lines: A Validated Panel for Preclinical Studies. Clin Cancer Res 25, 3141–3151 (2019). 10.1158/1078-0432.CCR-18-2953 [PubMed: 30737244]
19. Kessler BE et al. FAK Expression, Not Kinase Activity, Is a Key Mediator of Thyroid Tumorigenesis and Protumorigenic Processes. Mol Cancer Res 14, 869–882 (2016). 10.1158/1541-7786.MCR-16-0007 [PubMed: 27259715]
20. Obenauf AC et al. Therapy-induced tumour secretomes promote resistance and tumour progression. Nature 520, 368–372 (2015). 10.1038/nature14336 [PubMed: 25807485]
21. Dobin A. et al. STAR: ultrafast universal RNA-seq aligner. Bioinformatics 29, 15–21 (2013). 10.1093/bioinformatics/bts635 [PubMed: 23104886]
22. Anders S, Pyl PT & Huber W. HTSeq-a Python framework to work with high-throughput sequencing data. Bioinformatics 31, 166–169 (2015). 10.1093/bioinformatics/btu638 [PubMed: 25260700]
23. Torre D, Lachmann A. & Ma'ayan A. BioJupies: Automated Generation of Interactive Notebooks for RNA-Seq Data Analysis in the Cloud. Cell Syst 7, 556–561 e553 (2018). 10.1016/j.cels.2018.10.007 [PubMed: 30447998]
24. SEER Cancer Stat Facts: Thyroid Cancer. https://seer.cancer.gov/statfacts/html/thyro.html.
25. Li C, Lee KC, Schneider EB & Zeiger MA BRAF V600E mutation and Its Association with Clinicopathological Features of Papillary Thyroid Cancer: A Meta-Analysis. J Clin Endocr Metab 97, 4559–4570 (2012). 10.1210/jc.2012-2104 [PubMed: 23055546]
26. Byeon HK et al. Acquired resistance to BRAF inhibition induces epithelial-to-mesenchymal transition in BRAF (V600E) mutant thyroid cancer by c-Met-mediated AKT activation. Oncotarget 8, 596–609 (2017). 10.18632/oncotarget.13480 [PubMed: 27880942]
27. Huang F, Santinon F, Flores Gonzalez RE & Del Rincon SV Melanoma Plasticity: Promoter of Metastasis and Resistance to Therapy. Front Oncol 11, 756001 (2021). 10.3389/fonc.2021.756001 [PubMed: 34604096]
28. Stivarou T. & Patsavoudi E. Extracellular molecules involved in cancer cell invasion. Cancers (Basel) 7, 238–265 (2015). 10.3390/cancers7010238 [PubMed: 25629807]
29. Xin X, Khan ZA, Chen S. & Chakrabarti S. Extracellular signal-regulated kinase (ERK) in glucose-induced and endothelin-mediated fibronectin synthesis. Lab Invest 84, 1451–1459 (2004). 10.1038/labinvest.3700178 [PubMed: 15448709]
30. Sponziello M. et al. Fibronectin-1 expression is increased in aggressive thyroid cancer and favors the migration and invasion of cancer cells. Mol Cell Endocrinol 431, 123–132 (2016). 10.1016/j.mce.2016.05.007 [PubMed: 27173027]
31. Lanczky A. & Gyorffy B. Web-Based Survival Analysis Tool Tailored for Medical Research (KMplot): Development and Implementation. J Med Internet Res 23, e27633 (2021). 10.2196/27633 [PubMed: 34309564]
32. Lito P. et al. Relief of profound feedback inhibition of mitogenic signaling by RAF inhibitors attenuates their activity in BRAFV600E melanomas. Cancer Cell 22, 668–682 (2012). 10.1016/j.ccr.2012.10.009 [PubMed: 23153539]
33. Paraiso KH et al. Recovery of phospho-ERK activity allows melanoma cells to escape from BRAF inhibitor therapy. Br J Cancer 102, 1724–1730 (2010). 10.1038/sj.bjc.6605714 [PubMed: 20531415]
34. Cancer Genome Atlas Research, N. Integrated genomic characterization of papillary thyroid carcinoma. Cell 159, 676–690 (2014). 10.1016/j.cell.2014.09.050 [PubMed: 25417114]
35. Germann UA et al. Targeting the MAPK Signaling Pathway in Cancer: Promising Preclinical Activity with the Novel Selective ERK1/2 Inhibitor BVD-523 (Ulixertinib). Mol Cancer Ther 16, 2351–2363 (2017). 10.1158/1535-7163.MCT-17-0456 [PubMed: 28939558]
36. Schumacher S. et al. Structural insights into integrin alpha5beta1 opening by fibronectin ligand. Sci Adv 7 (2021). 10.1126/sciadv.abe9716
37. Liu C, Yao J, Mercola D. & Adamson E. The transcription factor EGR-1 directly transactivates the fibronectin gene and enhances attachment of human glioblastoma cell line U251. J Biol Chem 275, 20315–20323 (2000). 10.1074/jbc.M909046199 [PubMed: 10783396]

38. Gaggioli C. et al. HGF induces fibronectin matrix synthesis in melanoma cells through MAP kinase-dependent signaling pathway and induction of Egr-1. Oncogene 24, 1423–1433 (2005). 10.1038/sj.onc.1208318 [PubMed: 15608673]
39. Humphries MJ, Obara M, Olden K. & Yamada KM Role of fibronectin in adhesion, migration, and metastasis. Cancer Invest 7, 373–393 (1989). 10.3109/07357908909039866 [PubMed: 2531625]
40. Fedorenko IV, Wargo JA, Flaherty KT, Messina JL & Smalley KSM BRAF Inhibition Generates a Host-Tumor Niche that Mediates Therapeutic Escape. J Invest Dermatol 135, 3115–3124 (2015). 10.1038/jid.2015.329 [PubMed: 26302068]
41. Hirata E. et al. Intravital Imaging Reveals How BRAF Inhibition Generates Drug-Tolerant Microenvironments with High Integrin beta 1/FAK Signaling. Cancer Cell 27, 574–588 (2015). 10.1016/j.ccell.2015.03.008 [PubMed: 25873177]
42. Kenny HA et al. Mesothelial cells promote early ovarian cancer metastasis through fibronectin secretion. Journal of Clinical Investigation 124, 4614–4628 (2014). 10.1172/Jci74778 [PubMed: 25202979]
43. Nucera C, Lawler J. & Parangi S. BRAF(V600E) and microenvironment in thyroid cancer: a functional link to drive cancer progression. Cancer Res 71, 2417–2422 (2011). 10.1158/0008-5472.CAN-10-3844 [PubMed: 21447745]
44. Xia S. et al. Fibronectin 1 promotes migration and invasion of papillary thyroid cancer and predicts papillary thyroid cancer lymph node metastasis. Onco Targets Ther 10, 1743–1755 (2017). 10.2147/OTT.S122009 [PubMed: 28367057]
45. Gregg JL & Fraizer GC Transcriptional regulation of EGR1 by EGF and the ERK signaling pathway in prostate cancer. Cancer Research 71 (2011). 10.1158/1538-7445.Am2011-4013
46. Hoek KS et al. In vivo switching of human melanoma cells between proliferative and invasive states. Cancer Res 68, 650–656 (2008). 10.1158/0008-5472.CAN-07-2491 [PubMed: 18245463]
47. Li FZ, Dhillon AS, Anderson RL, McArthur G. & Ferrao PT Phenotype switching in melanoma: implications for progression and therapy. Front Oncol 5, 31 (2015). 10.3389/fonc.2015.00031 [PubMed: 25763355]
48. Spada S, Tocci A, Di Modugno F. & Nistico P. Fibronectin as a multiregulatory molecule crucial in tumor matrisome: from structural and functional features to clinical practice in oncology. J Exp Clin Cancer Res 40, 102 (2021). 10.1186/s13046-021-01908-8 [PubMed: 33731188]
49. Jailkhani N. et al. Noninvasive imaging of tumor progression, metastasis, and fibrosis using a nanobody targeting the extracellular matrix. Proc Natl Acad Sci U S A 116, 14181–14190 (2019). 10.1073/pnas.1817442116 [PubMed: 31068469]
50. Kumra H. & Reinhardt DP Fibronectin-targeted drug delivery in cancer. Adv Drug Deliv Rev 97, 101–110 (2016). 10.1016/j.addr.2015.11.014 [PubMed: 26639577]

Implications:

Together, these data show that increased invasion represents a new mechanism of resistance to BRAF inhibition in thyroid cancer that can be targeted with an ERK1/2 inhibitor.

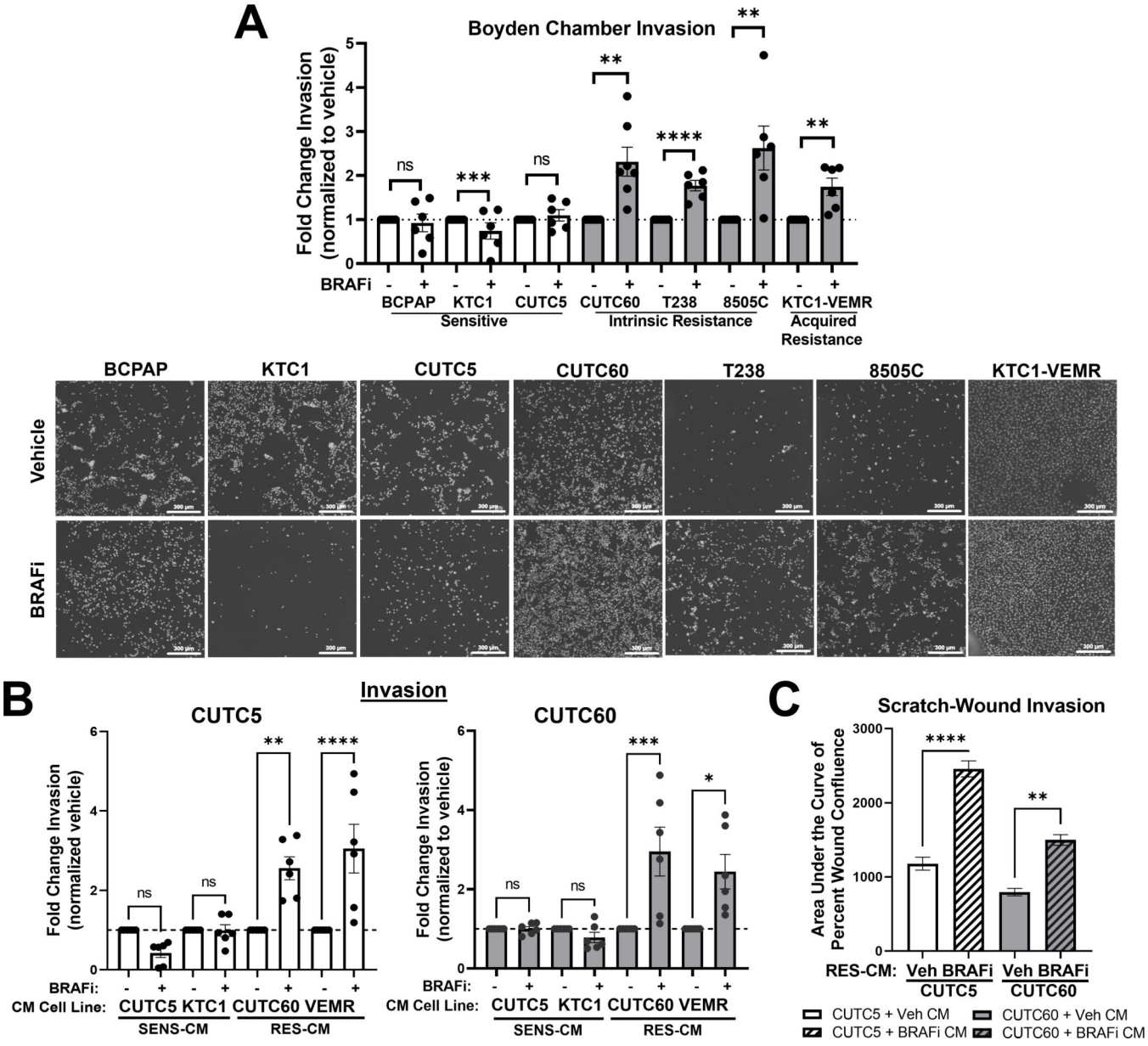

Figure 1. BRAFi-resistant, but not sensitive, cell lines exhibit a pro-invasive phenotype and secretome in response to BRAF inhibition.

A) BRAF-V600E cell lines that are sensitive (KTC1, CUTC5), have acquired resistance (KTC1-VEMR), or intrinsic resistance (T238, 8505C, CUTC60) to BRAF inhibition were treated with BRAFi for 24 hrs then plated in Matrigel-coated Boyden chambers for 24 hrs. Invading cells were stained with DAPI and counted using ImageJ or the Cytation 5 Cell Imaging Multi-Mode Reader. Representative images shown. **B)** CM was collected from sensitive (SENS-CM) or resistant (RES-CM) cell lines pre-treated with vehicle or BRAFi. BRAFi-sensitive or –resistant cell lines were treated with CM from indicated cell lines for 24 hrs then plated in Matrigel-coated Boyden chambers for 24 hrs, stained with DAPI and counted using ImageJ or the Cytation 5 Cell Imaging Multi-Mode reader. **A-B)** Results displayed as mean normalized to DMSO treated control. **C)** CUTC5 or CUTC60 cells

were plated in ImageLock 96-well plates, allowed to adhere overnight, scratched with a WoundMaker, then overlaid with Matrigel supplemented with CM from vehicle- or BRAFi-pretreated CUTC60 cells. Percent wound confluence was measured every 4 hrs for 72 hrs using IncuCyte® ZOOM live-cell imaging. Mean area under the curve of percent wound confluence over time +/− SEM. *, $p < 0.05$; **, $p < 0.01$; ***, $p < 0.001$; ****, $p < 0.0001$; ns = not significant. BRAFi: 100 nM dabrafenib, SENS-CM: conditioned media collected from BRAFi-sensitive cells, RES-CM: conditioned media collected from BRAFi-resistant cells.

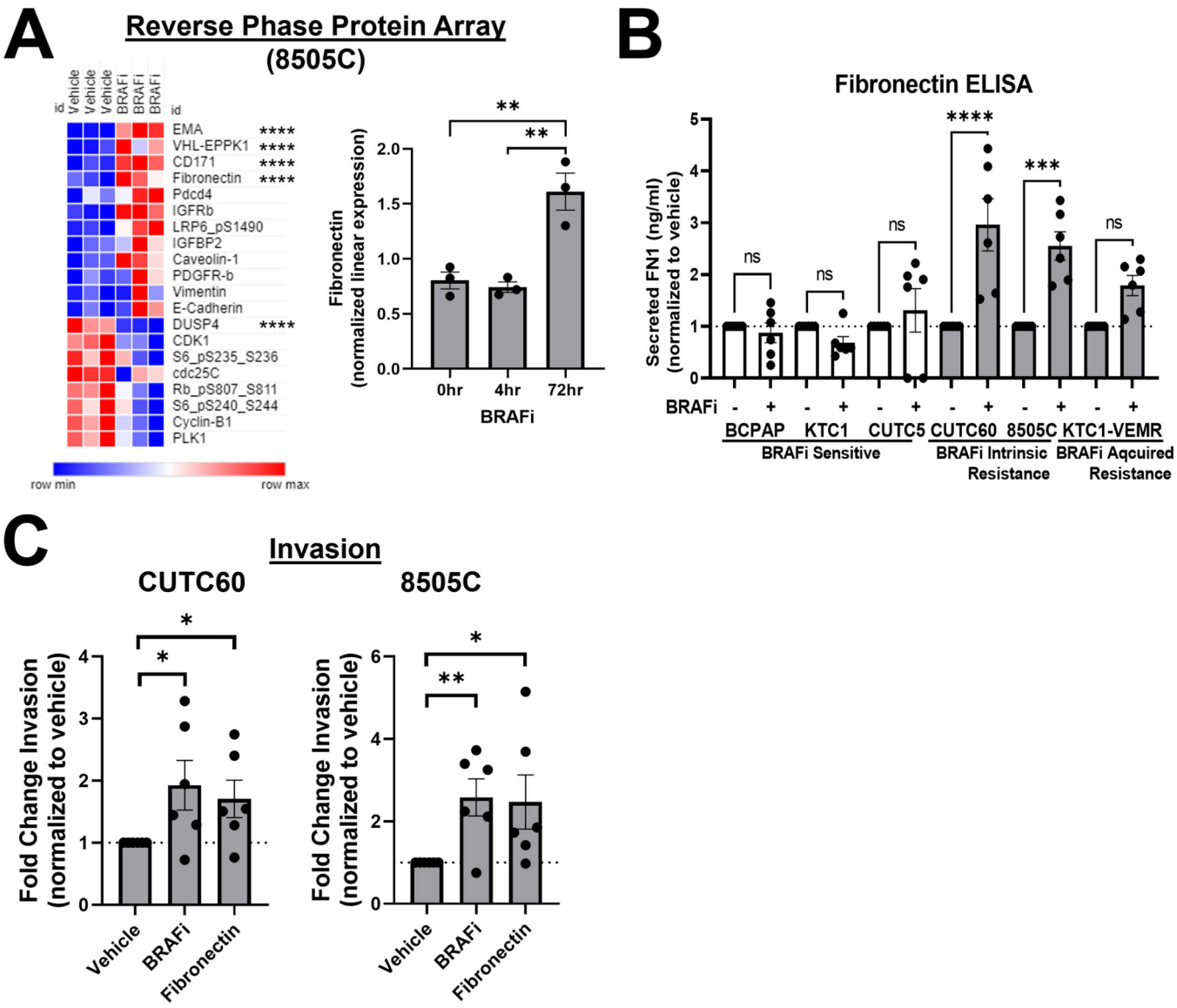

Figure 2. BRAF inhibition increases cellular and secreted fibronectin, which promotes invasion.

A) 8505C cells were treated with 1 μM vemurafenib for 4 or 72 hrs and protein expression was quantified using RPPA (MD Anderson Functional Proteomics Reverse Phase Protein Array Core). Heatmap generated using Morpheus. EMA/MUC1 (epithelial membrane antigen/mucin 1, VHL-EPPK1 (epiplakin 1), CD171 (cell adhesion molecule L1), FN1 (fibronectin), and DUSP4 (dual specificity phosphatase 4) are regulated most significantly. **B)** Cells were treated with vehicle or BRAFi for 72 hrs and secreted FN1 was quantified using ELISA assays (Invitrogen, Abcam). **C)** CUTC60 or 8505C cells were treated with either BRAFi or FN1 for 24 hrs, then plated in Matrigel-coated Boyden chambers and allowed to invade for 24 hrs. Invading cells were DAPI stained and quantified using ImageJ or the Cytation 5 Cell Imaging Multi-Mode Reader. Results displayed as mean +/− SEM. *, $p < 0.05$; **, $p < 0.01$; ***, $p < 0.001$; ****, $p < 0.0001$; ns = not significant. BRAFi: 1 μM vemurafenib or 100 nM dabrafenib, FN1: 100 ng/ml fibronectin.

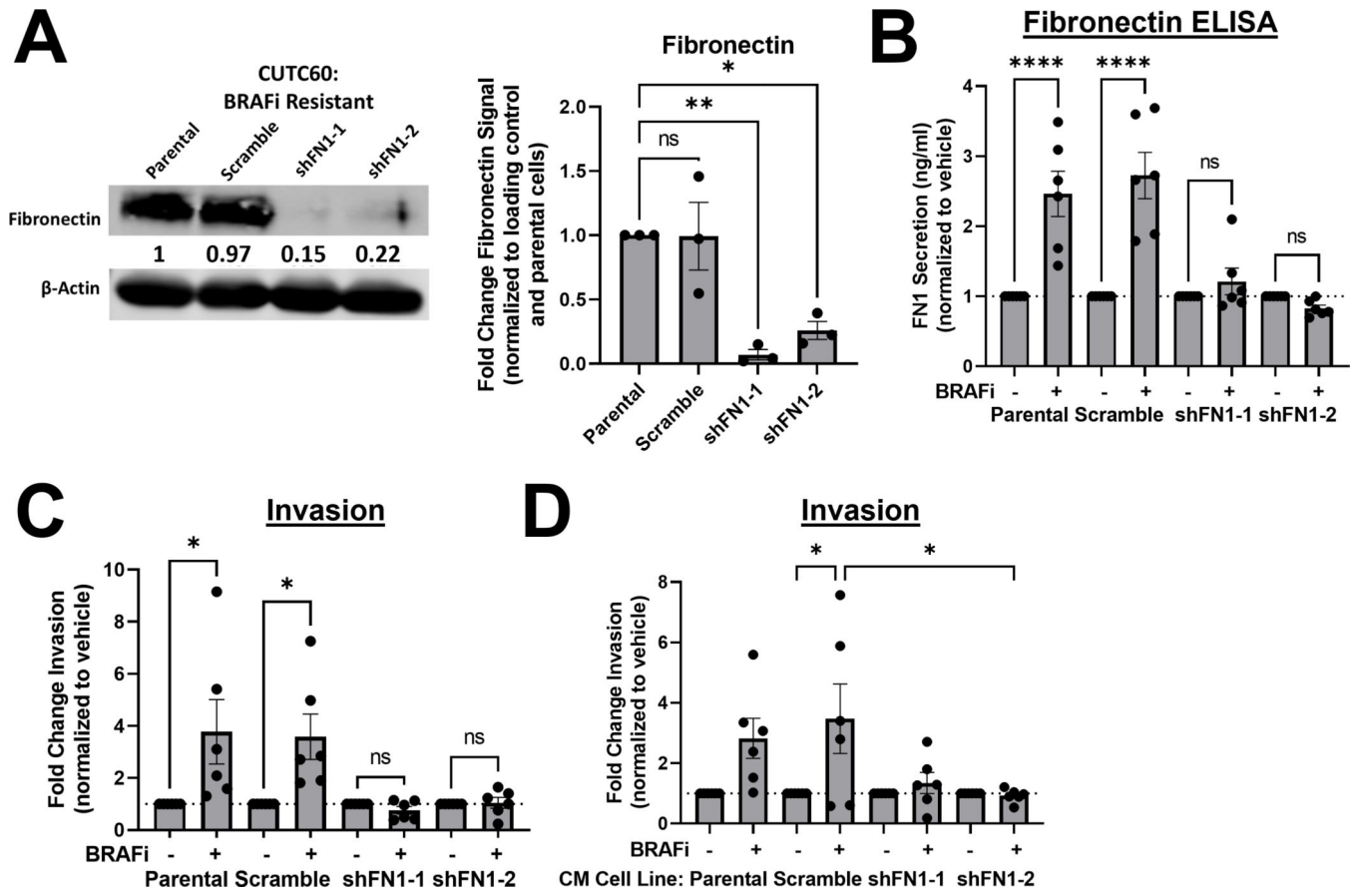

Figure 3. Fibronectin is necessary for a BRAFi-induced invasive phenotype.

A) FN1 was knocked down using shRNA in CUTC60 cells. Cell lysates were analyzed via western blot for indicated antibodies. **B)** CUTC60 cells were treated with vehicle or BRAFi for 72 hrs and secreted FN1 was quantified using ELISA assays (Invitrogen, Abcam). **C)** Indicated CUTC60 cells were treated with BRAFi for 24 hrs then plated in Matrigel-coated Boyden chambers for 24 hrs. Invading cells were stained with DAPI and counted using ImageJ or the Cytation 5 Cell Imaging Multi-Mode Reader. **D)** CM was collected from CUTC60 parental, scramble, or FN1 knockdown cell lines pre-treated with vehicle or BRAFi. BRAFi-sensitive or –resistant cell lines were treated with CM from indicated cell lines for 24 hrs then plated in Matrigel-coated Boyden chambers for 24 hrs, stained with DAPI and counted using the Cytation 5 Cell Imaging Multi-Mode Reader. Results displayed as mean +/− SEM. *, $p < 0.05$; ****, $p < 0.0001$; ns = not significant. BRAFi: 100 nM dabrafenib, FN1: fibronectin, CM: conditioned media.

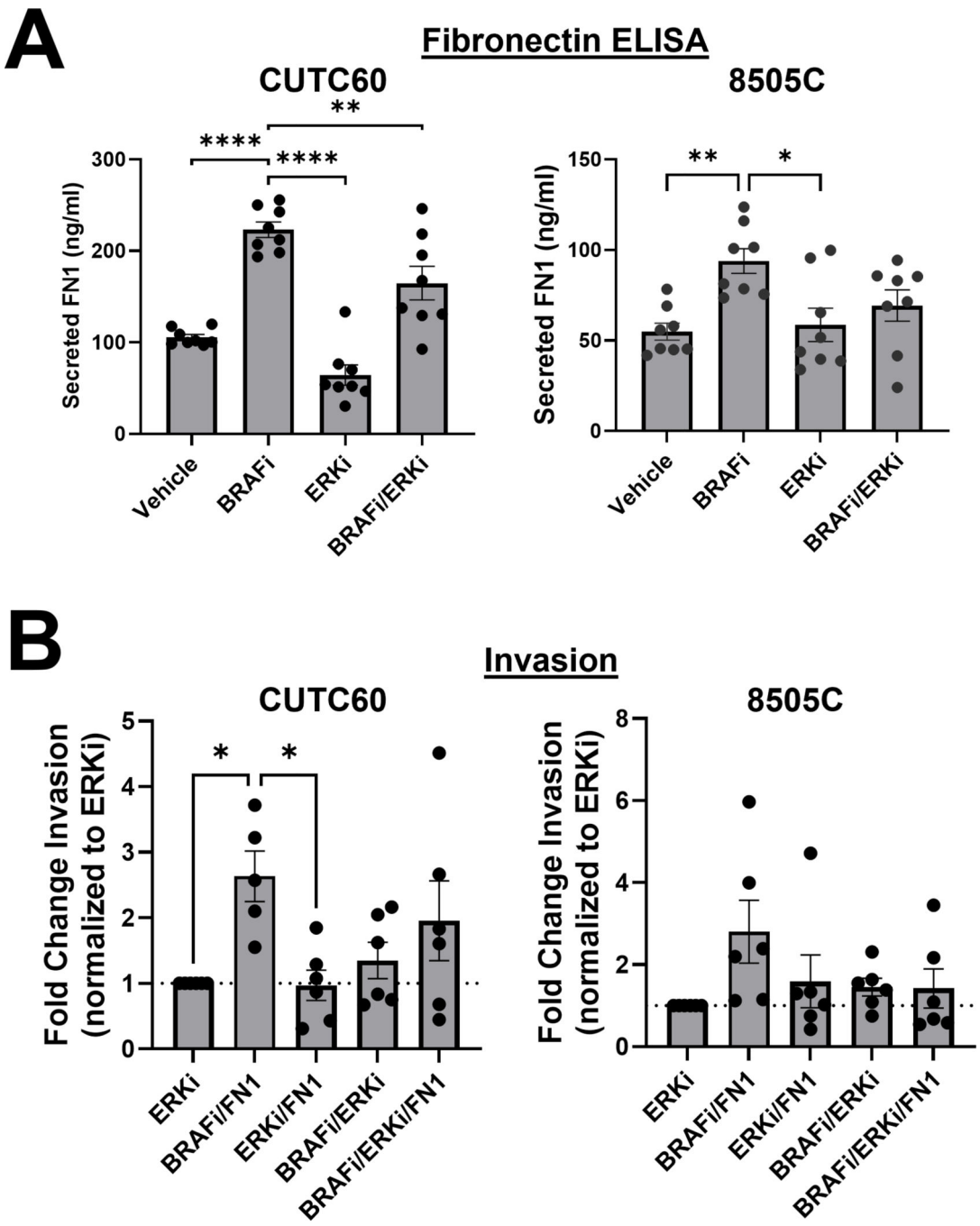

Figure 4. ERK1/2 inhibition can block an invasive phenotype in BRAFi-resistant cell lines.

A) Cells were treated with vehicle, BRAFi, ERKi, or the combination and secreted FN1 was quantified using ELISA assays **B)** Indicated cells were treated with BRAFi, ERKi, FN1, or the indicated combinations for 24 hrs then plated in Matrigel-coated Boyden chambers for 24 hrs. Invading cells were stained with DAPI and counted using ImageJ or the Cytation 5 Cell Imaging Multi-Mode Reader. Results displayed as mean +/− SEM. *, $p<0.05$; **, $p<0.01$. BRAFi: 100 nM dabrafenib, ERKi: 1 μM SCH772984, FN1: 100 ng/ml fibronectin.

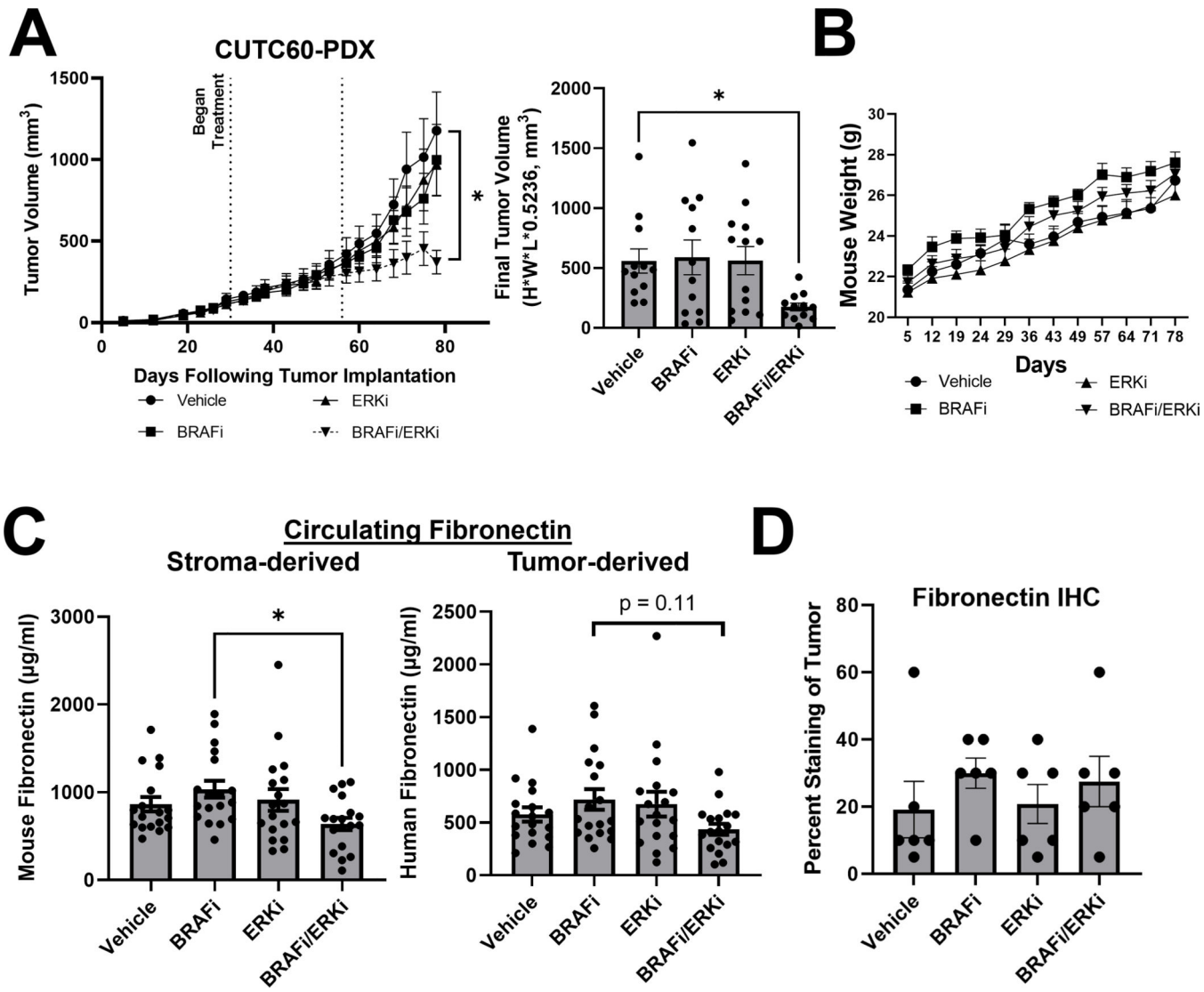

Figure 5. Combined BRAF and ERK1/2 inhibition reduces tumor growth and fibronectin *in vivo*.

A) Patient-derived xenograft (PDX) tumor chunks were injected into the flanks of athymic nude mice, allowed to grow to an average of 100mm^3, at which point treatment with vehicle, BRAFi, ERKi, or the combination was performed via oral gavage. After 30 days of treatment (day 55 post-injection), doses of BRAFi and ERKi were increased. **B)** Mice were weighed weekly. **C)** At the time of sacrifice, plasma was isolated from blood samples. Mouse-specific and human-specific FN1 ELISA assays (Abcam) were performed to distinguish between stroma-derived and tumor-derived circulating fibronectin, respectively. **D)** Immunohistochemistry was performed on tumor sections for FN1. Results displayed as mean +/− SEM. *, p<0.05. BRAFi: dabrafenib (30 mg/kg prior to day 55, 50 mg/kg post), ERKi: ulixertinib (50 mg/kg prior to day 55, 100 mg/kg post), FN1: fibronectin.

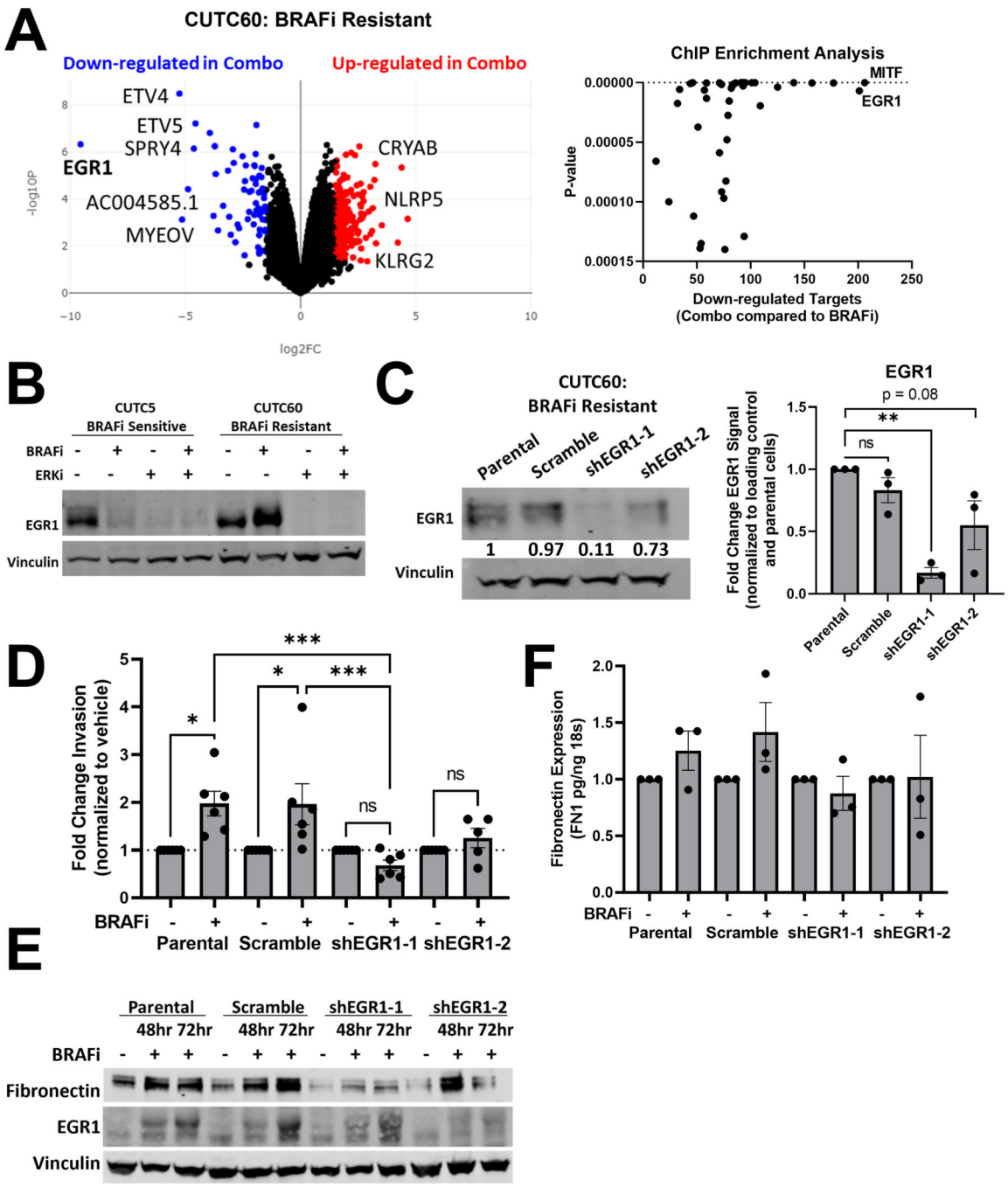

Figure 6: Combined BRAF and ERK1/2 inhibition decreases EGR1 levels and transcriptional targets.

A) RNA-sequencing was performed on CUTC60 cells treated with BRAFi, ERKi or the combination for 48 hrs (Anschutz Medical Campus Functional Genomics Core) and analyzed using BioJupies[25] to generate a volcano plot and perform ChIP Enrichment Analysis (CHEA). **B)** CUTC5 and CUTC60 cells were treated with BRAFi, ERKi or the combination for 48 hrs and western blots were performed for EGR1. **C)** In CUTC60 cells, EGR1 was knocked down using two shRNAs. Western blots were performed with indicated

antibodies. **D)** CUTC60 parental, scramble, or EGR1 knockdown cells were treated with vehicle or BRAFi for 24 hrs and plated in Matrigel-coated Boyden Chambers. After 24 hrs invading cells were stained with DAPI and counted. **E)** CUTC60 parental, scramble, or EGR1 knockdown cells were treated with BRAFi for 48 or 72hrs. Indicated proteins were analyzed via western blot. **F)** CUTC60 parental, scramble, or EGR1 knockdown cells were treated with vehicle or BRAFi for 48 hrs with a serum spike of 10% FBS in the final 1 hr of treatment. Quantitative PCR was performed using primers for FN1. Results displayed as mean normalized to control +/− SEM. *, $p < 0.05$; **, $p < 0.01$; ***, $p < 0.001$; ****, $p < 0.0001$; ns = not significant BRAFi: 100 nM dabrafenib, ERKi: 1 μM ulixertinib.

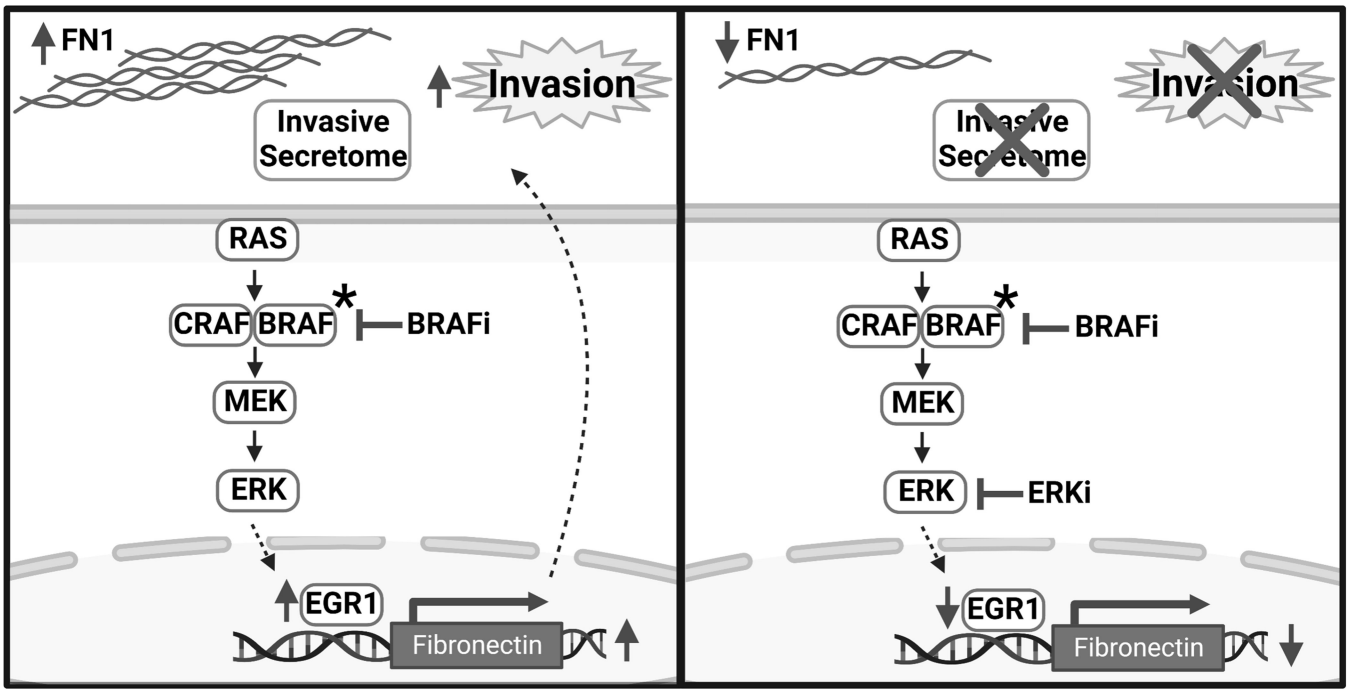

Figure 7. Model in which fibronectin contributes to a BRAF inhibitor-driven invasive phenotype through EGR1, which can be blocked by inhibition of ERK1/2.

In response to BRAF inhibition, thyroid cancer cells resistant to BRAFi become more invasive. This invasive phenotype is accompanied by an increase in FN1 and a pro-invasive secretome. Inhibition of ERK1/2 prevents BRAFi-induced FN1 secretion and corresponding invasive phenotype and secretome. Combined BRAF and ERK1/2 inhibition results in decreased levels of EGR1, which is necessary for increased FN1 expression in response to BRAFi. FN1: fibronectin. BRAFi: dabrafenib. ERKi: SCH772984 or ulixertinib. Created with BioRender.com